This leads to

$$w=\langle 0|V_0|0\rangle(E-W_0)[(E-W_0)^2+\epsilon^2]^{-1}, \quad (69a)$$

$$x=\int dW\langle W|V_0|W\rangle(E-W)[(E-W)^2+\epsilon^2]^{-1}, \quad (69b)$$

$$y=\oint dU\{(U|V_0|U)-(U|0\rangle\langle 0|V_0|U)\}(E-U) \times[(E-U)^2+\epsilon^2]^{-1}, \quad (69c)$$

$$z=\pi\{(E|V_0|E)-(E|0\rangle\langle 0|V_0|E)\}, \quad (69d)$$

where we have used the round bras and kets to represent the eigenstates of $H_0+Q\hat{K}\equiv\hat{H}_0$. In Eq. (69c) the symbol $\oint$ denotes that a sum over the discrete eigenstates of $\hat{H}_0$ is to be added to the integral over the continuum.

We see that the expressions for w, x, y, and z become more complicated in the BG treatment of this system than the corresponding expressions for the MM treatment. The relationship $k=k_1+k_2$ is not readily verified. However, it is apparent that $z(1-w+y)^{-1}$ will not in general vanish, so that there is no justification for the neglect of k_2.

ACKNOWLEDGMENTS

The authors are grateful to K. Kowalski, L. L. Foldy, and C. Bloch for helpful conversations.

PHYSICAL REVIEW VOLUME 163, NUMBER 4 20 NOVEMBER 1967

Shell-Model Theory of Nuclear Reactions in Deformed Nuclei*†

IRAJ R. AFNAN‡
Department of Physics and Laboratory of Nuclear Science, Massachusetts Institute of Technology, Cambridge, Massachusetts

(Received 10 April 1967)

A theoretical study has been made of the intermediate-structure resonances observed in neutron scattering and proton capture by F^{19} in terms of simple excitations of the compound nucleus using Feshbach's formalism for nuclear and photonuclear reactions. The simple excitations were taken to be particle-hole states in the deformed-level scheme, including the excitation of rotational bands. The average resonance widths, and spacing, and average total cross section ($\Delta E=0.5$ MeV) observed for $n+F^{19}$ with neutron energy between 0.5 and 2.5 MeV is reasonably well reproduced by the model. In particular, the agreement with the average total cross section indicates that an optical potential can be derived from the above model. In proton capture by F^{19}, though the calculated widths of the resonances are of the correct order of magnitude, the relative spacing of the resonances and magnitude of the cross sections is not in agreement with experiment.

I. INTRODUCTION

RECENT neutron-scattering experiments[1] have revealed resonances in average cross sections with widths ($\approx$200 keV) that are too large to be due to compound-nucleus formation, yet too small to be described by an optical model. It has been suggested[2–4] that such resonances might be due to the excitation of particularly simple states of the compound system. In light nuclei, we can hope to describe these simple excitations in terms of single-particle excitations (e.g., particle-hole states). Such calculations have already been performed for neutron scattering on N^{15} and C^{12},[5,6] using a particle-hole description for the excited states of the compound system. Widths of the order of 100–500 keV are obtained, in good agreement with experiment.

Another possible example of such intermediate structures, as these resonances have now been called, has been observed in neutron scattering on F^{19}.[7] In the same energy region above the ground state of Ne^{20} (16–20 MeV) the cross section for $F^{19}(p,\gamma)Ne^{20}$ is known[8] and manifests resonances of a similar nature to the observed structure in $n+F^{19}$. We take the point of view that the appearance of similar resonance structure

* This work is supported in part through funds provided by the U. S. Atomic Energy Commission under Contract No. AT(30-1) 2098.

† Based in part on the author's Ph.D. thesis, MIT, Cambridge, Massachusetts, 1966 (unpublished).

‡ Present address: Physics Department, University of Minnesota, Minneapolis, Minnesota.

[1] E. S. Elwyn, J. E. Monahan, R. Q. Lane, and F. P. Mooring, Argonne National Laboratory Summer Report No. ANL 7081, 1965, p. 24 (unpublished).

[2] A. K. Kerman, L. S. Rodberg, and J. E. Young, Phys. Rev. Letters **11**, 422 (1963).

[3] H. Feshbach, A. K. Kerman, and R. H. Lemmer, Ann. Phys. (N. Y.) **41**, 230 (1967).

[4] B. Block and H. Feshbach, Ann. Phys. (N. Y.) **23**, 47 (1963).

[5] R. H. Lemmer and C. M. Shakin, Ann. Phys. (N. Y.) **27**, 13 (1964).

[6] I. Lovas, Nucl. Phys. **81**, 353 (1966).

[7] J. E. Monahan, Bull. Am. Phys. Soc. **11**, 451 (1966); A. J. Elwyn, J. E. Monahan, R. O. Lane, and A. Langsdorf, Jr., Nucl. Phys. **59**, 113 (1964); J. E. Monahan and A. J. Elwyn, Phys. Rev. **153**, 1148 (1967).

[8] N. W. Tanner, G. C. Thomas, and E. D. Earle, Nucl. Phys. **52**, 29 (1964); S. S. Hanna, in Proceedings of the Summer Study on the Physics of the Emperor Tandem Van de Graaff Region, Brookhaven National Laboratory Report No. BNL 948(C-46), 1965 (unpublished).

in different reaction channels (here $n+F^{19}$ and $\gamma+Ne^{20}$) leading to compound states of the $A=20$ system is an indication that this structure does not have a statistical origin.[9]

The present investigation is thus a theoretical study of the cross section for the above two reactions, using a suitable nuclear model for the $A=20$ compound system. The interest in such a calculation is to see if the mechanism of simple excitations (in this case particle-hole excitations), give the correct number of resonances, and nucleon and γ-ray widths that are in agreement with experimental widths.

In Sec. II we summarize some results of Feshbach's formalism for nuclear reactions, which will be used throughout the investigation. We then proceed in Sec. III to discuss the structure of the target nucleus F^{19}, and the compound system $A=20$, in the light of the nuclear model we will be using. Since the low-energy spectrum of both Ne^{20} and F^{19} indicates that these nuclei are probably deformed, we will have to incorporate this deformation into our model. Section IV presents the numerical results and their comparison with experimental results. Comparison of the calculated results with the experiment indicates:

1. In the reaction $n+F^{19}$, the calculated particle widths, and average spacing of levels is in agreement with the experimental results. This suggests that the model we have used has the right number of degrees of freedom, and the mechanism of excitation used to evaluate the neutron widths gives a rather good description of the physical process.

2. The calculated average neutron cross section, using an averaging interval of 0.5 MeV, agrees very well with the observed average cross section, showing that the model is capable of giving a good estimate of the strength function $\langle\Gamma\rangle/\langle D\rangle$. This also means that we can calculate an optical potential from the model that will correctly reproduce the average experimental cross section over the energy range under consideration (0 to 2.5 MeV neutron energy).

3. The calculated differential cross section for $F^{19}(p,\gamma)Ne^{20}$ is in poor agreement with experiment, indicating that the model fails to reproduce the more detailed properties of the system when interference effects between different partial waves became important.

II. REACTION THEORY

There are a number of different formalisms for nuclear reactions. We have found Feshbach's version the most convenient for our particular problem. In this section we will briefly present the main results we need of that formalism for nuclear reactions. For details refer to the original papers of Feshbach.[10]

[9] R. E. Segel, Z. Vager, L. Meyer-Schützmeister, P. P. Singh, and R. G. Allas, Nucl. Phys. **A93**, 33 (1967).

[10] H. Feshbach, Ann. Phys. (N. Y.) **5**, 357 (1958); **19**, 287 (1962); H. Feshbach and L. Estrada, *ibid.* **23**, 123 (1963).

Introducing the projection operators P and Q on the open and closed channels, respectively, we get a set of coupled equations for the closed and open channels. These coupled equations can be solved to give a transition amplitude for going from an initial state β to a final state α of the form

$$T_{\alpha\beta}=T_{\alpha\beta}(\text{pot}) +\langle\psi_\alpha^{(-)}|H_{PQ}\frac{1}{E-H_{QQ}-W_{QQ}}H_{QP}|\psi_\beta^{(+)}\rangle, \quad (1)$$

where $T_{\alpha\beta}(\text{pot})$ is the transition amplitude for potential scattering. The states $\psi_\alpha^{(\pm)}$ are the scattering solutions to the average field the incident nucleon observes in channel α. The interaction H_{QP} and H_{PQ} connect the open and closed channels. The operator W_{QQ} is given by

$$W_{QQ}=H_{QP}\frac{1}{E^{(+)}-H_{PP}}H_{PQ} =H_{QP}\frac{\mathcal{P}}{E-H_{PP}}H_{PQ}-i\pi H_{QP}\delta(E-H_{PP})H_{PQ}, \quad (2)$$

where $\mathcal{P}$ is the Cauchy principal value. The operator H_{QQ} is an $(A+1)$ particle Hamiltonian for the closed channels. In the case of one isolated resonance Eq. (1) reduces to

$$T_{\alpha\beta}=T_{\alpha\beta}(\text{pot})+\frac{\langle\psi_\alpha^{(-)}|H_{PQ}|\Phi_n\rangle\langle\Phi_n|H_{QP}|\psi_\beta^{(+)}\rangle}{(E-E_n-\Delta_n)+\frac{1}{2}i\Gamma_n}, \quad (3)$$

where

$$\Delta_n=\langle\Phi_n|H_{QP}\frac{\mathcal{P}}{E-H_{PP}}H_{PQ}|\Phi_n\rangle, \quad (4a)$$

$$\Gamma_n=2\pi\langle\Phi_n|H_{QP}\delta(E-H_{PP})H_{PQ}|\Phi_n\rangle, \quad (4b)$$

$$H_{QQ}\Phi_n=E_n\Phi_n. \quad (5)$$

The second term in (3) is the standard one-level Breit-Wigner transition amplitude. In the case of overlapping resonances, since W_{QQ} is complex and not diagonal in the eigenstates of H_{QQ}, we have to solve a complex eigenvalue problem. However, when the separation D between the eigenstates of H_{QQ} is large compared to the widths Γ_n of these states, the transition amplitude can be approximated by

$$T_{\alpha\beta}=T_{\alpha\beta}(\text{pot})+\sum_n\frac{\langle\psi_\alpha^{(-)}|H_{PQ}|\Phi_n\rangle\langle\Phi_n|H_{QP}|\psi_\beta^{(+)}\rangle}{(E-E_n-\Delta_n)+\frac{1}{2}i\Gamma_n}, \quad (6)$$

where Δ_n and Γ_n are given by (4a) and (4b), respectively. We write the scattering state $\psi_\alpha^{(\pm)}$ in an angular momentum representation as

$$\psi_{ljI}{}^{J(+)}=e^{i\delta_{lj}}\frac{V_{lj}(r)}{r}|(ls)jI;JM\rangle, \quad (7)$$

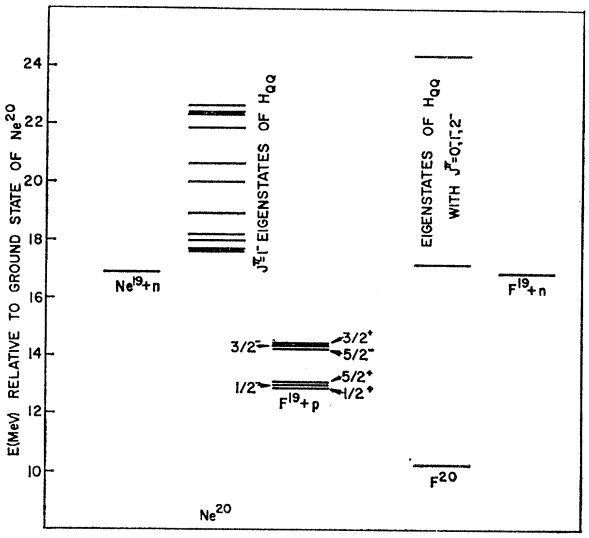

FIG. 1. The energy of all the nuclei and the threshold of the channels we are dealing with relative to the ground state of Ne^{20}. The ground state of F^{20} and $n+F^{19}$ threshold has been pushed up so that the eigenstates of H_{QQ} with $T=1$, $T_3=1$ are at the same energy as the states with $T=1$, $T_3=0$. This way all the eigenvalue of H_{QQ} can be referred to the ground state of Ne^{20}. In Ne^{20} we have indicated the eigenstates of H_{QQ} with $J^\pi=1^-$. In F^{20} we have indicated the region in which the calculated eigenstates of H_{QQ} with $J^\pi=0^-, 1^-, 2^-$ are presented. We have also indicated the low-lying spectrum of F^{19}.

where we have coupled the total angular momentum of the incident particle j, to the target spin I to get the total angular momentum J. In (7), δ_{lj} is the phase shift due to the potential the incident particle feels. Taking $T_{\alpha\beta}(\text{pot})$ to be the transition amplitude for potential scattering we get, for the total transition amplitude,

$$T_{ljI;\,l'j'I'}{}^J=\frac{-1}{\pi}e^{i\delta_{lj}}\sin\delta_{lj}\delta_{ll'}\delta_{jj'}\delta_{II'}+\sum_n\frac{e^{i\delta_{lj}}g_{ljI}{}^J(n)g_{l'j'I'}{}^J(n)e^{i\delta_{l'j'}}}{(E-E_n-\Delta_n{}^J)+\frac{1}{2}i\Gamma_n{}^J}, \quad (8)$$

where

$$\begin{aligned}\Gamma_n{}^J&=2\pi\langle\Phi_n{}^J|H_{QP}\delta(E-H_{PP})H_{PQ}|\Phi_n{}^J\rangle\\&=2\pi\sum_{ljI}|\langle\Phi_n{}^J|H_{QP}|\psi_{ljI}{}^J\rangle|^2\\&=2\pi\sum_{ljI}|g_{ljI}{}^J(n)|^2=\sum_{ljI}\Gamma_{ljI}{}^{J,n}.\end{aligned} \quad (9)$$

In the above, all scattering states $\psi_{ljI}{}^J$ must be energy-normalized. The total cross section is given in terms of the transition amplitude as[11]

$$\sigma_T=\frac{4\pi^3}{k_i^2}\frac{1}{(2s_i+1)(2I_i+1)}\sum_{\alpha i\alpha f,fJ}(2J+1)|T_{\alpha f\alpha i}{}^J|^2, \quad (10)$$

where s_i and I_i are the spins of the incident particle and target nucleus, respectively, and α stands for the channel quantum numbers (l,j). Using Eqs. (8) and (10) we obtain the average total cross section in an energy interval ΔE, in terms of the strength function $\langle\Gamma_\alpha{}^J\rangle/\langle D^J\rangle$, as

$$\langle\sigma_T\rangle=\frac{2\pi}{k_i^2}\sum_J\frac{(2J+1)}{(2s_i+1)(2I_i+1)}\times\sum_{\alpha i}\left\{1-\cos2\delta_{\alpha_i}\left(1-\pi\frac{\langle\Gamma_{\alpha_i}{}^J\rangle}{\langle D^J\rangle}\right)\right\}. \quad (11)$$

Since we will be evaluating the strength function and the average cross section for neutron energy between 0.5 and 2.5 MeV, we have defined the strength functions for a given channel α and total angular momentum J as

$$\frac{\langle\Gamma_\alpha{}^J\rangle}{\langle D^J\rangle}=\frac{1}{\Delta E}\sum_n\Gamma_\alpha{}^{J,n}. \quad (12)$$

The transition amplitude for photoproduction is derived in the same manner as Eq. (8) to get

$$T_{\alpha,ljI}{}^J=\langle\psi_\alpha|H^{N\gamma}|\psi_{ljI}{}^{J(+)}\rangle+\sum_n\frac{\langle\psi_\alpha|H^{N\gamma}|\Phi_n{}^J\rangle\langle\Phi_n{}^J|H_{QP}|\psi_{ljI}{}^{J(+)}\rangle}{(E-E_n-\Delta_n{}^J)+\frac{1}{2}i\Gamma_n{}^J}, \quad (13)$$

where $H^{N\gamma}$ is the dipole operator and is given by

$$\begin{aligned}H^{N\gamma}&=-ie(2\pi\hbar\omega)^{1/2}\sum_{j=1}^{A}\left(\tfrac{1}{2}-\tau_{3j}-\frac{Z}{A}\right)\boldsymbol{\varepsilon}\cdot\mathbf{r}_j\\&=C\mathbf{D}\cdot\boldsymbol{\varepsilon},\end{aligned} \quad (14)$$

after removing the contribution coming from center-of-mass motion. The symbols are: $C=-ie(2\pi\hbar\omega)^{1/2}$, $\boldsymbol{\varepsilon}$ is the polarization of the photon, and τ_{3j} is the third component of isotopic spin. Introducing an operator $T_\mu{}^1$ as

$$T_\mu{}^1=D_\mu{}^1+\sum_n\frac{D_\mu{}^1|\Phi_n{}^J\rangle\langle\Phi_n{}^J|H_{QP}}{(E-E_n-\Delta_n{}^J)+\frac{1}{2}i\Gamma_n{}^J}, \quad (15)$$

we can then write the differential cross section for proton capture as

$$\frac{d\sigma}{d\Omega}(p,\gamma)=\frac{(2\pi)^2(\hbar\omega)^3e^2}{\hbar c(2M_pc^2)E_p}\sum_L B_LP_L(\mathbf{k}_p\cdot\boldsymbol{\varepsilon}), \quad (16)$$

where

$$B_L=\frac{1}{24\pi(2I_i+1)}\sum_{\tilde{\alpha}\tilde{J},\alpha J}\langle\alpha J||T^1||I_f\rangle\langle\tilde{\alpha}\tilde{J}||T^1||I_f\rangle^*\times\begin{Bmatrix}L&\tilde{J}&J\\I&j&\tilde{j}\end{Bmatrix}i^{l-\tilde{l}}(-1)^{S_f+I_i-I_f}Z(lj\tilde{l}\tilde{j};\tfrac{1}{2}L)\times Z(1\tilde{J}1J;I_fL), \quad (17)$$

where $\hbar\omega$ is the energy of the photon, M_p and E_p are

[11] See, for example, R. H. Lemmer, Rept. Progr. Phys. **39**, 131 (1966).

the reduced mass and energy of the incident proton, and I_i and I_f are the spins of the target and final nucleus, respectively. In the above, the proton wave functions are again energy-normalized; the function $Z(abcd; ef)$ is defined by Biedenharm *et al.*[12] as

$$Z(abcd; ef) = i^{f-a+c}[(2a+1)(2b+1)(2c+1)(2d+1)]^{1/2} \times W(abcd; ef)(a0c0|acf0).$$

III. THE NUCLEAR MODEL

As seen in the last section the calculation of the transition amplitude requires the knowledge of the states Φ_n. The states Φ_n are the eigenstates of the Hamiltonian H_{QQ}, which is an $(A+1)$ particle Hamiltonian. To get the complete spectrum of H_{QQ} is an impossible task. We therefore, have to resort to a nuclear model that will give us an approximate wave function Φ_n. It is in terms of this nuclear model that the simple excitations are described. Actually, we are not interested in the complete spectrum of the $(A+1)$-particle Hamiltonian, but that part of the spectrum that is connected to the open channels via H_{QP}. It is this part of the spectrum of H_{QQ} that gives by definition the simple excitations of the compound nucleus. Since the Φ_n we use in the calculation are model wave functions which depend on the nucleus we are dealing with, it means that the simple excitation depends on that. In the case we will be dealing with, both collective and particle-hole excitations are included in simple configurations of the compound system. In this section we will discuss the model to be employed for the target system F^{19} and the compound system of $A=20$.

The F^{19} target: The low-lying spectrum of F^{19} is presented in Fig. 1. The positive parity states indicate that F^{19} is deformed in its ground state, since the two states of $\frac{5}{2}^+$ and $\frac{3}{2}^+$ can be described as part of the rotational band on top of the ground state. In discussing F^{19} as a deformed nucleus we must look at the Nilsson scheme (Fig. 2). At large deformation, we observe a large gap ≈ 5 MeV between the lowest $\frac{1}{2}^+$ and the next state of $\frac{3}{2}^+$. This immediately indicates that we can describe F^{19}, which has two neutrons and one proton outside the O^{16} core, as a hole in the $\frac{1}{2}^+$ level. The negative parity state of $\frac{1}{2}^-$ in F^{19} can be described as an excitation of the hole into the $\frac{1}{2}^-$. Though the Nilsson scheme gives the right spin for the $\frac{1}{2}^-$ as a hole in the p shell, it does not give the right energy. However, we do not expect the Nilsson scheme to give us very good single-particle energies. Taking the $\frac{1}{2}^-$ to be a hole in the p shell, we then evaluate, using the rotational model, the energies of the $\frac{3}{2}^-$ and $\frac{5}{2}^-$. We find that the agreement between the calculated and observed energies is very good. However, there is a disagreement in the energies of the positive parity band. This can be due to the coupling of these states with a positive parity rotational band at higher

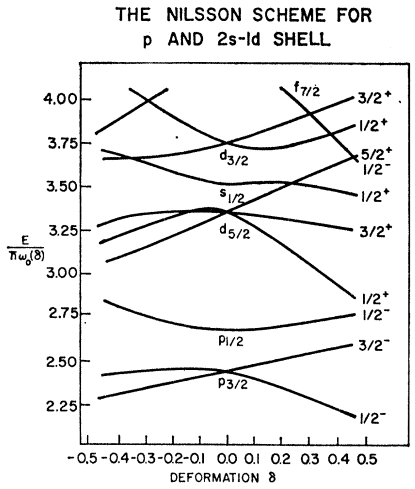

FIG. 2. The Nilsson scheme for $1p$ and $2s$-$1d$ shell.

energy via the Coriolis coupling. Since we will be interested in the cross section for $n+F^{19}$ up to neutron energies of 2 MeV, we will have to consider the six states of F^{19} in Fig. 1 as open channels. Thus, the open channels can be defined as a hole in either the lowest $\frac{1}{2}^+$ state in the $2s$-$1d$ shell or the highest $\frac{1}{2}^-$ state in the p shell plus the rotational bands on top of these intrinsic states. Using the above model for F^{19}, we can write the wave function of the target nucleus as $D_{mk}{}^I\chi_{kq}$, where $D_{mk}{}^I$ is the representation of the rotation group and is defined by

$$\psi_{IM}(\mathbf{r}) = \sum_{M'} D_{MM'}{}^I(\alpha\beta\gamma)\psi_{IM'}(\mathbf{r}'), \tag{18}$$

where $\psi_{IM}(\mathbf{r})$ is in the space-fixed coordinates, while $\psi_{IM'}(\mathbf{r}')$ is in the body-fixed coordinates. χ_{kq} is the intrinsic wave function of the system in the body-fixed coordinates. In the case of F^{19}, χ_{kq} is the state of the hole in either the $\frac{1}{2}^+$ or the $\frac{1}{2}^-$ Nilsson levels. On proper symmetrization of the above wave function, we get for the target state

$$|I_h M_h k_h q_h\rangle = \left(\frac{2I_h+1}{16\pi^2}\right)^{1/2} \{D_{M_h k_h}{}^{I_h}\chi_{-k_h q_h} + (-1)^{I_h+\pi_h-\frac{1}{2}} D_{M_h -k_h}{}^{I_h}\chi_{k_h q_h}\}, \tag{19}$$

where π_h is the parity of the state χ_{kq}, which is given by

$$\chi_{k_h q_h} = \sum_{l_h j_h} C_{l_h j_h}{}^{q_h - k_h}(-1)^{j_h - k_h} a_{l_h j_h k_h}|0\rangle, \tag{20}$$

where $a_{l_h j_h k_h}$ is the destruction operator for a particle in state (l_h, j_h, k_h) and $C_{l_h j_h}{}^{q_h - k_h}$ are the coefficients of the Nilsson expansion. Thus the target state is described as a hole in either the lowest $\frac{1}{2}^+$ state in the $2s$-$1d$ shell or the highest $\frac{1}{2}^-$ state in $1p$ shell, with the rotational bands on top of these intrinsic states.

The $A=20$ system: We turn now to the discussion of the compound system which is formed when a proton

[12] L. C. Biedenharm and J. M. Blatt, Rev. Mod. Phys. 24, 249 (1952).

or neutron is scattered by F^{19}. If we have a nucleon incident on F^{19}, the incident nucleon will interact with nucleons in the target via a two-body interaction. This two-body interaction can cause the incident nucleon to drop into a bound state while one of the nucleons in the p shell will gain the energy lost by the incident nucleon and fill the $\frac{1}{2}^+$ hole, i.e., particle-hole excitations are produced. We may expect the average field in which these particle-hole states are made to be deformed also. The ground state of the $A=20$ system is Ne^{20}. Ne^{20} has a rotational band on top of the ground state with $K=0$,[13] where K is the projection of the total angular momentum along the axis of symmetry. The existence of rotational bands in the low-lying spectrum of Ne^{20} indicates that Ne^{20} is deformed in its ground state. However, we are going one step further in assuming that the average field that the particle-hole states feel is also deformed. This is a strong assumption, for it is difficult to say that the average nuclear field will keep the same deformation when we excite states with energy of 20 MeV. However, because of the lack of any better nuclear model, we keep the same deformation for the excited states as in the ground state. Furthermore, taking different deformation for the excited states, and ground state introduces complications in the orthogonality of the projection operators P and Q. Thus, the simple excitations that we are considering are particle-hole states in a deformed scheme. To write the state Φ_n in terms of the above nuclear model, we have to define that part of the space spanned by the particle-hole state that will contribute to Φ_n. Φ_n is an eigenstate of H_{QQ} and thus should not have any open channel component in it. We defined the open channels by a hole in the lowest $\Omega=\frac{1}{2}^+$ state in the $2s$-$1d$ shell and the highest $\Omega=\frac{1}{2}^-$ state in the p shell. Thus, the particle-hole states we will consider should have the hole in any of the p-shell states with the exception of the highest $\Omega=\frac{1}{2}^-$, while the particle is in any of the unoccupied states in the $2s$-$1d$ shell. This assures the orthogonality of the projection operators P and Q, which was made use of in formulating the reaction theory presented in Sec. II. The Hamiltonian H_{QQ} has two parts. The first is the unperturbed diagonal particle-hole energies. The second part is a residual two-body interaction which is taken to be the same as the two-body interaction used by Brown *et al.*[14] It is given by

$$V_{ij}=-V_0[a+b\boldsymbol{\sigma}_i\cdot\boldsymbol{\sigma}_j]\delta(\mathbf{r}_i-\mathbf{r}_j), \tag{21}$$

where $a=0.865$, $b=0.135$, $V_0=4\pi p^3\times 8.5$ MeV, where $p=1.76$ F.

Having defined the Hamiltonian H_{QQ}, we diagonalize this Hamiltonian in the particle-hole basis defined above, to get the states $\Xi_{K,S}$. Taking the eigenstates of H_{QQ} to have good total isotopic spin (T,T_3), we get

$$\Xi_{K,S}{}^{T,T_3}=\sum_{q_p\Omega_p,\,q_h\Omega_h} A_{q_p\Omega_p;\,q_h\Omega_h}{}^{K,S} \times[a_{q_p\Omega_p}{}^{\dagger}a_{q_h\Omega_h}]_{T_3}{}^{T}|0\rangle, \tag{22}$$

where $a_{q_p\Omega_p}{}^{\dagger}$ and $a_{q_h\Omega_h}$ are the creation and annihilation operators for a nucleon, respectively, and the bracket indicates the coupling of the particle-hole state to a total isotopic spin (T,T_3). The coefficients $A_{q_p\Omega_p;\,q_h\Omega_h}{}^{K,S}$ are obtained from the diagonalization of H_{QQ} in the particle-hole basis. Because of the fact that our average field is deformed, there is a collective degree of freedom that we have not taken into consideration. Thus H_{QQ} has to include a part that defines this collective motion. We therefore, add to H_{QQ}, the Hamiltonian for a rotor, and the eigenstates of H_{QQ} are now written as $D_{MK}{}^{J}\times\Xi_{KS}{}^{TT_3}$. Thus the normalized and symmetrized eigenstates of H_{QQ} are written as

$$|JMKS:TT_3\rangle=\left(\frac{2J+1}{16\pi^2}\right)^{1/2}\{D_{MK}{}^{J}\Xi_{KS}{}^{TT_3} +(-1)^{J+\pi_{\rm ph}+1}D_{M-K}{}^{J}\Xi_{-KS}{}^{TT_3}\}, \tag{23}$$

where $D_{MK}{}^{J}$ is the representation of the rotation group, and $\pi_{\rm ph}$ is the parity of the particle-hole states, which are negative in our case. The states $\Xi_{-K,S}{}^{TT_3}$ are defined as

$$\Xi_{-KS}{}^{TT_3}=\sum_{\Omega_p q_p,\,\Omega_h q_h} A_{q_p\Omega_p;\,q_h\Omega_h}{}^{KS} \times[a_{q_p-\Omega_p}{}^{\dagger}a_{q_h-\Omega_h}]_{T_3}{}^{T}|0\rangle. \tag{24}$$

Thus the eigenstates of H_{QQ} consist of linear combinations of particle-hole states, with rotational bands on top of these intrinsic states. We will find later that the extra collective degrees of freedom are necessary to get the right density of states. In the above, we have ignored the coupling due to the Coriolis force between states of different K.

To be able to evaluate the widths $\Gamma_s{}^{J}$, we have to know the spectrum of eigenstates of H_{PP}. To obtain these states we have to use the model we described for the target nucleus, and introduce an average field that the incident particle sees. Since our target nucleus is deformed, we take this deformation into consideration, and write

$$H_{PP}=T+U+H_A \tag{25}$$

for H_{PP}, where T is the kinetic energy of the incident nucleon. U is the average field of the target seen by the incident nucleon, and H_A is the Hamiltonian of the target nucleus. Since the target nucleus is deformed, we take U to be a deformed well. This deformation will couple different partial waves so that Eq. (7) becomes

$$\psi_{ljI}{}^{J}=\sum_{l'j'I'}\frac{1}{r}V_{ljI;\,l'j'I'}{}^{J}|(l's)j'I';JM\rangle. \tag{26}$$

The ket $|(ls)jI;JM\rangle$ consists of coupling the incident

[13] H. C. Evans *et al.*, Can. J. Phys. **43**, 83 (1965).
[14] G. E. Brown, L. Castillejo, and J. A. Evans, Nucl. Phys. **22**, 1 (1961).

particle's total angular momentum j with the target spin I to get the total angular momentum (JM).

The radial function $V_{ljI;l'j'I'}{}^{J}$ is obtained by solving a set of coupled equations, where the coupling is due to the deformation of the average field U. The deformation couples partial waves of the same parity, e.g., the s and d waves will be coupled. In the energy region we are interested in, the dominant partial waves are the s, p, and d waves. Since our states Φ_n have negative parity, only p waves feed the eigenstates of H_{QQ}. However, these states Φ_n can decay, leaving the nucleus in an excited negative parity state and the important partial waves in this case are the s and d waves. For the present calculation, we ignore the coupling between the s and d wave. This allows us to write (26) as

$$\psi_{ljI}{}^{J}=\frac{1}{r}V_{ljI}{}^{J}(r)\,|\,(ls)jI;\,JM\rangle.$$

Introducing the isotopic spin of the incident particle and the target nucleus and coupling these to a total isotopic spin (T,T_3), we get for the scattering eigenstates of H_{PP}

$$\psi_{ljIk}{}^{JT}=\frac{1}{r}V_{ljI}{}^{JT}(r)\sum_{mm_j}(jm_jIm\,|\,JM)\times\sum_{\tau\tau_h}(-1)^{\frac{1}{2}-\tau_h}(\tfrac{1}{2}\tau\tfrac{1}{2}-\tau_h\,|\,TT_3)Y_{ljm_j}\eta_\tau\left(\frac{2I+1}{16\pi^2}\right)^{1/2}\times\{D_{MK}{}^{I}\chi_{-kq_h}{}^{\tau_h}+(-1)^{I+\pi-\frac{1}{2}}D_{m-k}{}^{I}\chi_{kq_h}{}^{\tau_h}\},\quad(27)$$

where we have used the target wave function as given by Eq. (19). Y_{ljm_j} is the angular part of the incident particle wave function and η_τ is the isotopic spinor for the incident nucleon.

Having developed a nuclear model for the target nucleus and the compound system of $A=20$, and obtaining explicit expressions for the eigenstates of H_{QQ} and H_{PP}, we can proceed to evaluate the transition amplitudes and cross sections for the reaction. The particular case we are considering is the scattering of a nucleon by F^{19}. We see that the incident nucleon can go, via the deformation and two-body interaction, either to a state that is a linear combination of particle-hole states without any rotation of the system, or to a linear combination of the particle-hole states and rotate the system at the same time. If we look at the decay of the eigenstates of H_{QQ}, and if the system is not rotating, it can decay by emission of a nucleon, leaving the target either rotating or not rotating. If the system is rotating when in the compound state, then it can decay by particle emission, leaving the target nucleus either rotating or in its ground state.

So far, we have been discussing the formation of the eigenstates of H_{QQ} from the open channels and their final decay back into the open channels. We notice that we can get to all the eigenstates of H_{QQ} from the open channels, provided angular-momentum selection rules do not prohibit the transition. Our approach ignores any effects coming from the coupling of the Φ_n to more complicated modes of excitation in the compound system. We know, for example, that in deformed nuclei, the Coriolis force can play a very important role, as in the case of the ground-state band of F^{19}. The Coriolis force in this case couples states that differ by $\Delta K=\pm1$. This means that the different rotational bands that have $\Delta K=\pm1$ are connected. Thus, if the Coriolis coupling is strong, we can come in from the open channels into the states say, $J=1$, $K=0$. This state will either go into a state of $J=1, K=1$, through the Coriolis coupling, or decay into the open channels, depending on the lifetime of the state and the strength of the coupling. We have not taken such effects into consideration. Another process that we have ignored that can effect the width is the decay of the particle-hole state to two-particle two-hole ($2p$-$2h$) states and more complicated configurations.

IV. NUMERICAL CALCULATION AND RESULTS

Having described a formalism for nuclear reactions and the model for the nuclei we will be dealing with, we proceed to evaluate the cross section for neutron scattering by F^{19} and proton capture by F^{19}. Both of these reactions lead to compound states in the $A=20$ system. The states that we reach from the open channels are negative parity states,[15] since these states were taken as linear combinations of particle-hole states with the particle in the $2s$-$1d$ shell and the hole in the p shell. The states in the $A=20$ system that we get via $n+F^{19}$ have a total isotopic spin $T=1$, $T_3=+1$. These we consider to be the analog states to the states we get in proton capture, which have an isotopic spin $T=1$, $T_3=0$ (see Fig. 1).

The spectrum of these $T=1$ negative parity states are obtained by diagonalizing the intrinsic part of H_{QQ} in the particle-hole basis, and then adding rotational bands on top of these intrinsic states. The intrinsic part of H_{QQ} consists of two parts. The first part, which is diagonal in the particle-hole basis, is the unperturbed energy of the particle-hole states. These diagonal terms are usually taken from the experimental spectrum of the adjoining nuclei, because these energies can be obtained theoretically, only by solving the many-body problem. In the nuclei we are dealing with, these energies cannot be extracted from experiments and we have obtained them from our nuclear model. We will find

[15] We have not considered the even-parity $2p$-$2h$ states with two holes in the lowest $\frac{1}{2}^+$ level of the $2s$-$1d$ shell, and two particles in any of the other states of the $2s$-$1d$ shell, even though these states are connected to the open channel via H_{QP}. The reasons for not taking these states into consideration are: First, these states do not couple to the negative parity states; second, when we adjust the diagonal particle-hole energies these even-parity states will probably be bound.

later on that these energies obtained from the model have to be modified slightly to get agreement with experiments. But this is expected, for we know that the nuclear model we have chosen will not give us particle-hole energies that agree with experiments. The second part of H_{QQ}, which is not diagonal in the particle-hole basis, is the residual particle-hole interaction given by Eq. (21). To diagonalize H_{QQ}, we have to evaluate the matrix elements of V_{ij} between particle-hole states, and that is given by

$$\langle (N_p\Omega_p q_p)(N_h\Omega_h q_h)^{-1}T=1,\ T_3|\,V\,|(N_p'\Omega_p' q_p')(N_h'\Omega_h' q_h')T=1,\ T_3\rangle=\sum_{j_p l_p, j_p' l_p'}\ \sum_{j_h l_h, j_h' l_h'}(-1)^{j_h-\Omega_h+j_h'-\Omega_h'}C_{l_p j_p}{}^{q_p\Omega_p}$$

$$\times C_{l_h j_h}{}^{q_h-\Omega_h}C_{l_p' j_p'}{}^{q_p'\Omega_p'}C_{l_h' j_h'}{}^{q_h'-\Omega_h'}V_0F_0[(2j_p+1)(2j_h+1)(2j_p'+1)(2j_h'+1)]^{1/2}(-1)^{\Omega_p'-\Omega_h'}$$

$$\times\Bigg\{(a-b)\sum_{l=\text{even}}(2l+1)\begin{pmatrix} j_p' & l & j_p\\ -\Omega_p' & \Omega_p'-\Omega_p & \Omega_p\end{pmatrix}\begin{pmatrix} j_h' & l & j_h\\ -\Omega_h' & \Omega_h'-\Omega_h & \Omega_h\end{pmatrix}\begin{pmatrix} j_p' & l & j_p\\ \frac{1}{2} & 0 & -\frac{1}{2}\end{pmatrix}\begin{pmatrix} j_h' & l & j_h\\ \frac{1}{2} & 0 & -\frac{1}{2}\end{pmatrix}$$

$$+2b(-1)^{\Omega_h'-\Omega_p}\sum_{l=\text{odd}}(2l+1)\begin{pmatrix} j_h & l & j_p\\ -\Omega_h & \Omega_h-\Omega_p & \Omega_p\end{pmatrix}\begin{pmatrix} j_h' & l & j_p'\\ -\Omega_h' & \Omega_h'-\Omega_p' & \Omega_p'\end{pmatrix}\begin{pmatrix} j_h & l & j_p\\ \frac{1}{2} & 0 & -\frac{1}{2}\end{pmatrix}\begin{pmatrix} j_h' & l & j_p'\\ \frac{1}{2} & 0 & -\frac{1}{2}\end{pmatrix}\Bigg\}, \quad (28)$$

where

$$F_0=\frac{1}{4\pi}\int_0^\infty R_{N_h l_h}R_{N_h' l_h'}R_{N_p l_p}R_{N_p' l_p'}\frac{dr}{r^2}, \quad (29)$$

with R_{Nl} the radial harmonic-oscillator wave functions. The $C_{lj}{}^{q\Omega}$ are the coefficients involved in the expansion

$$\chi_{\Omega q}=\sum_{lj}C_{lj}{}^{q\Omega}\chi_{lj\Omega},$$

where $\chi_{\Omega q}$ are the single-particle states in an average deformed well and these states are not eigenstates of total angular momentum but are eigenstates of the projection of angular momentum along the axis of symmetry of the system. $\chi_{lj\Omega}$ are states of good total angular momentum and its projection along the symmetry axis, and are the single-particle states in a spherical average field.

Having evaluated the matrix elements of H_{QQ} in the particle-hole basis, we diagonalize that matrix to get the spectrum of the intrinsic part of H_{QQ}. However, before we can perform this diagonalization we have to get the coefficients $C_{lj}{}^{q\Omega}$. These coefficients can be obtained in one of two ways. The first is by taking them as Nilsson coefficients, which involves taking an anisotropic harmonic oscillator as the deformed well and expanding its eigenstates in terms of spherical harmonic-oscillator states. The second method is to take these coefficients from a restricted Hartree-Fock[16] (HF) calculation, where $C_{lj}{}^{q\Omega}$ are used as variational parameters to minimize the energy. In Fig. 3 we have the single-particle spectrums from both the HF and Nilsson scheme. The parameters used in the Nilsson scheme for the harmonic oscillator are the same as the ones used by Nilsson,[17] i.e., $\omega_0=41/A^{1/3}=15.1$ MeV for $A=20$. The strength of the spin-orbit interaction was taken as $c=-2.4$ MeV, and the strength of the l^2 term was taken to be zero. The deformation of $\delta=0.4$ was taken. This deformation was obtained from the experimental $B(E2)$ transition to the ground state of Ne^{20} on the basis of a rotational model.

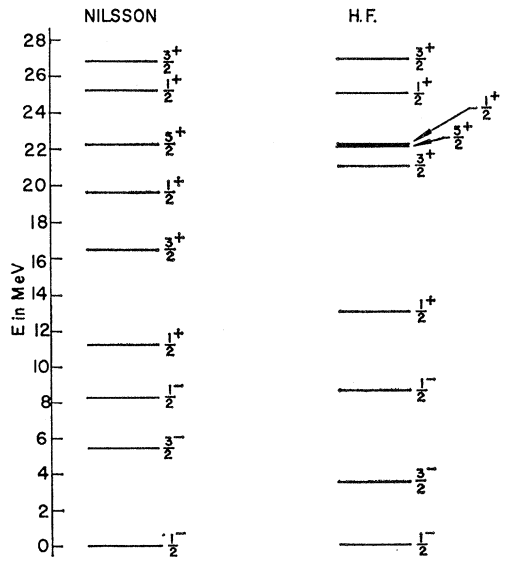

FIG. 3. Single-particle levels in Hartree-Fock scheme, and the Nilsson scheme with deformation $\delta=0.4$.

We see in Fig. 3 that there is a gap between the occupied and unoccupied states. This justifies our taking particle-hole states. However, this gap is larger in the HF scheme than in the Nilsson scheme. Actually, this gap remains in the HF scheme as we go to other even-even nuclei, while in the Nilsson scheme this gap disappears. We also know that the HF method is a self-consistent method, while the Nilsson scheme chooses a phenomenological potential. We then proceed to get the spectrum of H_{QQ} in both of these schemes. We find that the HF states are all above threshold for $n+F^{19}$,

[16] I. Kelson, Phys. Rev. **132**, 2189 (1963); I. Kelson and C. A. Levinson, *ibid.* **134**, B269 (1964); W. H. Bassichis, C. A. Levinson, and I. Kelson, *ibid.* **136**, B380 (1964); W. H. Bassichis, and F. Schick (to be published).

[17] S. G. Nilsson, Kgl. Danske Videnskab. Selskab, Mat.-Fys. Medd. **29**, No. 16 (1955).

which is 16.815 MeV with respect to the ground state of Ne^{20}. The Nilsson states, on the other hand, have states below threshold. We also observe that when the channels in which the residual nucleus has negative parity are opened, the states with lowest energy in the HF disappear from the spectrum, while this is not the case in the Nilsson scheme. We therefore, have decided to choose the HF for the rest of the calculation. Adding the rotational band to the intrinsic states, we get the complete spectrum of H_{QQ}, which is presented in Fig. 4. Since the intrinsic part of the Hamiltonian H_{QQ} is invariant under the group RR_2 (i.e., rotation about the intrinsic z axis and reflections in the intrinsic x-z plane), there the intrinsic states Ξ_K transform irreducebly under RR_2. For $K=0$ there are two representations of the group RR_2.[18] The first representation has states Ξ_0 that are odd under reflection through the intrinsic x-z plane and have rotational bands with angular momentum $J^\pi=0^-, 2^-, 3^-, \cdots$. Thus, in Fig. 4, though there are eight $K=0$ states, only four states have even angular momentum while the other four states have odd angular momentum. The energy scale in Fig. 4 is chosen such that the zero of the energy is the threshold for the reaction $n+F^{19}$. We have not included states with $J>2$, since we cannot get to these states through the entrance channel because of angular-momentum selection rules.

Having obtained the spectrum of H_{QQ}, we turn our attention to the evaluation of the widths. From Eq. (9) we have for the partial width $\Gamma_{ljIk}{}^{n,J}$

$$\Gamma_{ljIk}{}^{n,J}=2\pi|\langle\Phi_n{}^J|H_{QP}|\psi_{ljIk}{}^J\rangle|^2 =2\pi|g_{ljIk}{}^J(n)|^2. \tag{30}$$

Making use of Eqs. (21) and (25), we can evaluate the above matrix element to get, for $T=1$,

$$\begin{aligned}\langle\Phi_n{}^J|H_{QP}|\psi_{ljIk}{}^J\rangle=&\sum_{\Omega_p q_p,\,\Omega_h q_h} A_{q_p\Omega_p;\,q_h\Omega_h}{}^{K,n}\sum_{l_pj_pl_hj_h,\,l_h'j_h'}(-1)^{j_h-\Omega_h+j_h'+k}C_{l_pj_p}{}^{q_p\Omega_p}C_{l_hj_h}{}^{q_h-\Omega_h}C_{l_h'j_h'}{}^{q_h'k}\\
&\times(-1)^{I-j}V_0F_1[(2I+1)(2j_p+1)(2j_h+1)(2j_h'+1)(2j+1)]^{1/2}\Big[(a-b)\sum_{l'}(2l'+1)\tfrac14\{1+(-1)^{l_p+l'+l}\}\\
&\times\{1+(-1)^{l_h+l'+l_h'}\}\begin{pmatrix}j_p & l' & j\\ \frac12 & 0 & -\frac12\end{pmatrix}\begin{pmatrix}j_h' & l' & j_h\\ \frac12 & 0 & -\frac12\end{pmatrix}\Big\{\begin{pmatrix}j_p & l' & j\\ -\Omega_p & \Omega_h+k & K-k\end{pmatrix}\begin{pmatrix}j_h' & l' & j_h\\ k & -\Omega_h-k & \Omega_h\end{pmatrix}\\
&\times\begin{pmatrix}j & I & J\\ K-k & k & K\end{pmatrix}+(-1)^{j_h'+I}\begin{pmatrix}j_p & l' & j\\ -\Omega_p & \Omega_h-k & K+k\end{pmatrix}\begin{pmatrix}j_h' & l' & j_h\\ -k & k-\Omega_h & \Omega_h\end{pmatrix}\begin{pmatrix}j & I & J\\ K+k & -k & -K\end{pmatrix}\Big\}\\
&+2b(-1)^{k+\Omega_p}\sum_{l'}(2l'+1)\tfrac14\{1+(-1)^{l_p+l'+l_h}\}\{1+(-1)^{l_h'+l'+l}\}\begin{pmatrix}j_p & l' & j_h\\ \frac12 & 0 & -\frac12\end{pmatrix}\begin{pmatrix}j_h' & l' & j\\ \frac12 & 0 & -\frac12\end{pmatrix}\begin{pmatrix}j_p & l' & j_h\\ -\Omega_p & K & \Omega_h\end{pmatrix}\\
&\times\Big\{\begin{pmatrix}j_h' & l' & j\\ k & -K & K-k\end{pmatrix}\begin{pmatrix}j & I & J\\ K-k & k & -K\end{pmatrix}-(-1)^{j_h'+I}\begin{pmatrix}j_h' & l' & j\\ -k & -K & K+k\end{pmatrix}\begin{pmatrix}j & I & J\\ K+k & -k & -K\end{pmatrix}\Big\}\Big],\end{aligned} \tag{31}$$

where

$$F_1=\frac{1}{4\pi}\int_0^\infty R_{N_pl_p}R_{N_hl_h}R_{N_h'l_h'}V_{lj}\frac{dr}{r^2}. \tag{32}$$

To evaluate the above integral we have to choose a potential well to get $V_{lj}(r)$. The potential we have taken is a Woods-Saxon potential of the form

$$V(r)=-V_0\rho(r)+V_{so}\left(\frac{\hbar}{M_\pi c}\right)^2\frac{1}{r}\frac{d\rho(r)}{dr}(\boldsymbol{\sigma}\cdot\mathbf{l}), \tag{33}$$

where

$$\rho(r)=\left[1+\exp\left(\frac{r-R}{a}\right)\right]^{-1}, \tag{34}$$

and

$$a=0.7\text{ F}, \qquad R=3.32\text{ F},$$
$$V_{so}=6.85\text{ MeV}, \quad V_0=50.5\text{ MeV}.$$

The depth of 50.5 MeV was determined so that the potential scattering cross section agreed with the measured cross section for $n+F^{19}$ at low energy[19] and in regions where the cross section does not manifest any resonances.

In the case when the projectile is a proton, we add to the above potential the Coulomb potential due to a uniform charge sphere of radius R. To get the proton width, we use the same procedure as for a neutron width, with the exception that the continuum radial wave function $V_{lj}(r)$ is given by a Woods-Saxon plus Coulomb potential.

If we look at the phase shifts for both protons and neutrons in the above potential we find that the $d_{3/2}$ proton partial wave goes through resonances at 3.0 MeV, while the neutron $d_{3/2}$ state is bound. Actually, none of the neutron partial waves resonate below an energy of 3.0 MeV, which is the region of interest.

[18] I am grateful to Professor B. Bayman for drawing my attention to this point.

[19] C. T. Hibdon, Phys. Rev. **133**, B353 (1964).

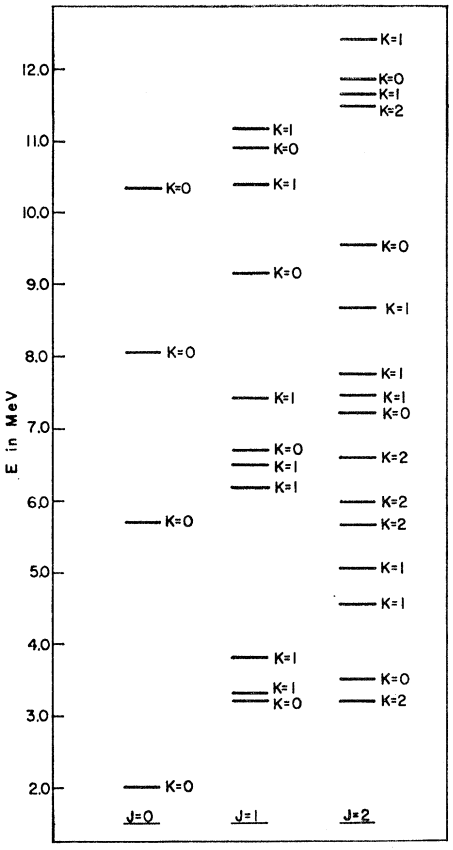

FIG. 4. Calculated eigenstates of H_{QQ} with $J^\pi=0^-$, 1^-, 2^-. The energy is measured with respect to the threshold of $n+F^{19}$.

Though the proton $d_{3/2}$ partial wave resonates, in the region where the experiment is performed, which is 4.0–8.0 MeV proton incident energy, there is no potential scattering resonance. The reason for stressing the lack of potential scattering resonances is because in the region of potential scattering resonance, the widths $\Gamma_n{}^J$ are strongly enhanced and the approximation we made to get Eq. (6) fails.

Having obtained the spectrum of H_{QQ} and the widths of the eigenstates of H_{QQ} to the continuum, we turn our attention to the evaluation of the total cross section for $n+F^{19}$. In Fig. 5 we show the measured cross section between 0.5 and 2.5 MeV with a resolution of 15–20 keV.[7] This cross section has been averaged with different averaging intervals up to $\Delta E=380$ keV. We see that with $\Delta E\sim 95$ keV there are four resonances in the cross section with widths between 100–200 keV. We want to see if our mechanism of excitation of the compound system will produce the same number of resonances with widths and average spacing of the same order of magnitude.

As we increase the energy of the incident neutrons from 0.5 to 2.5 MeV the number of open channels is increased. The open channels are defined by the energy, spin, parity, and the partial waves for each state of the target nucleus. From Fig. 1 we see that at an incident neutron energy of 0.5 there are 3 open channels, while at an energy of 2.5, we have six open channels.

From Eq. (8) we have for the real part and the imaginary part of the transition amplitude

$$\mathrm{Re}(T_{\alpha_f\alpha_i}{}^{JT})=-\frac{1}{\pi}\sin\delta_{\alpha_i}\cos\delta_{\alpha_i}\delta_{\alpha_i,\alpha_f}$$
$$+\sum_n \frac{g_{\alpha_f}{}^{JT}(n)g_{\alpha_i}{}^{JT}(n)}{(E-E_n)^2+(\frac{1}{2}\Gamma_n{}^{JT})^2}\{(E-E_n)\cos(\delta_{\alpha_i}+\delta_{\alpha_f})$$
$$+\tfrac{1}{2}\Gamma_n{}^{JT}\sin(\delta_{\alpha_i}+\delta_{\alpha_f})\}, \quad (34')$$

and

$$\mathrm{Im}(T_{\alpha_f\alpha_i}{}^{JT})=-\frac{1}{\pi}(\sin\delta_{\alpha_i})^2\delta_{\alpha_i,\alpha_f}$$
$$+\sum_n \frac{g_{\alpha_f}{}^{JT}(n)g_{\alpha_i}{}^{JT}(n)}{(E-E_n)^2+(\frac{1}{2}\Gamma_n{}^{JT})^2}\{(E-E_n)\sin(\delta_{\alpha_i}+\delta_{\alpha_f})$$
$$-\tfrac{1}{2}\Gamma_n{}^{JT}\cos(\delta_{\alpha_i}+\delta_{\alpha_f})\}, \quad (34'')$$

where α_i and α_f define the incident channel and exit channels. δ_{α_i} and δ_{α_f} are the phase shifts due to H_{PP} for the partial waves in the incident and exit channels, respectively. The $\Gamma_n{}^{JT}$ is the total width for a given state Φ_n, while E_n is the corresponding eigenvalue.

If we look at the spectrum of H_{QQ} (Fig. 4), we see that there are no states below 2 MeV, while the experimental cross section manifests resonances below 2 MeV. The calculated 1^- states are centered around an energy of 25 MeV above the ground state of Ne^{20}, while the proton capture cross section (Fig. 6)[8] indicates that the giant

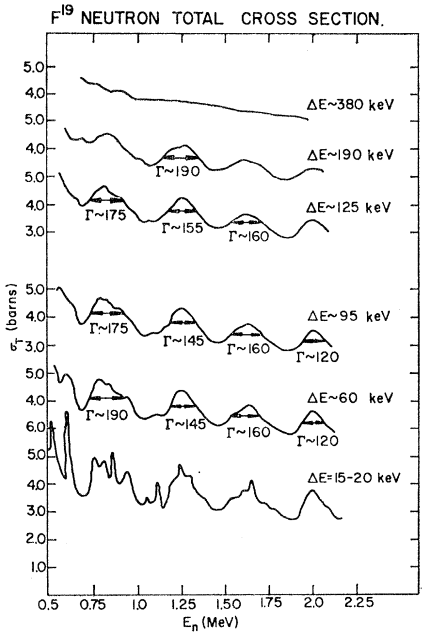

FIG. 5. Measured F^{19} neutron total cross section (Refs. 1 and 7).

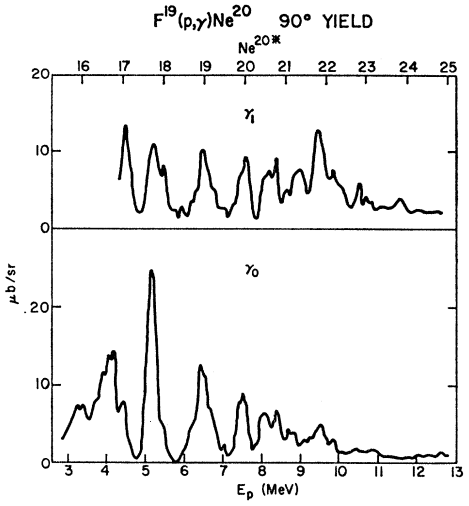

FIG. 6. The measured differential cross section for $F^{19}(p,\gamma_0)Ne^{20}$ and $F^{19}(p,\gamma_1)Ne^{20*}$ at 90° (Ref. 8).

dipole resonance is centered at an excitation energy of 20 MeV. This indicates that the calculated spectrum of H_{QQ} should be lowered by ≈ 5 MeV in order that the center of the giant dipole resonance will coincide with the center of the 1^- states. This is equivalent to the adjustment of the diagonal particle-hole energies, which in most calculations of this kind are from experiments. Unfortunately, in our case the experimental particle-hole energies are not available. Using Eqs. (34′) and (34″) and (10) ,we can evaluate the total cross section for $n+F^{19}$. In Fig. 7 we present the calculated and experimental neutron total cross section for $n+F^{19}$. The eigenvalues of H_{QQ} were lowered by 5.35 MeV to fit the resonance at 0.8 MeV. In evaluating the neutron cross section, the matrix elements $g_\alpha{}^{JT}(s)$ and δ_α were calculated at energy intervals of 0.25 between zero and 2.5 MeV. A linear extrapolation was then set up for both $g_\alpha{}^{JT}(s)$ and δ_α to get the energy dependence of both quantities into the cross section.

In Table I we present all the eigenstates of H_{QQ}, their quantum number, and their elastic and total width. To see why only five of the states in Table I show up as resonances in the total cross section, consider a Breit–

TABLE I. Energy, spin, total widths, and elastic widths of the states calculated in $n+F^{19}$ between 0.5 and 3.0 MeV neutron energy.

E_s (MeV)	J	K	Γ^{Js} (keV)	$\Gamma_i{}^{Js}$ (keV)
0.6219	2	2	13.5	10.6
0.8466	1	1	109	52.5
1.1524	1	1	72	23.5
1.2376	2	2	58	33
1.369	1	0	388	129.5
1.85	2	0	202	83
2.083	1	1	158	14
2.0966	2	1	174.5	4.2
2.4024	2	1	244	122
2.7096	0	0	124.5	12

TABLE II. Experimental (19) and calculated spins, and energies of resonances in $n+F^{19}$ in the energy region between 0.5 and 2.5 MeV neutron energy.

E (calc)	E (exp)	J^π (exp)	J^π (calc)
0.8	0.8	1^-	1^-
1.15	1.15	1^-	1^-
1.24	...	...	2^-
1.85	1.70	0^-	2^-
2.4	1.95	0^-	2^-

Wigner-type transition amplitude for an isolated resonance. The total resonance cross section has then the following energy dependence:

$$\sigma_T \propto \frac{\Gamma_i{}^{JT}(n)\Gamma_n{}^{JT}}{(E-E_n)^2+(\frac{1}{2}\Gamma_n{}^{JT})^2},$$

where $\Gamma_i{}^{JT}(n)$ is the width for the elastic channel for the state (J,T,n), while $\Gamma_n{}^{JT}$ is the total width for that state. At resonance, the above expression reduces to

$$\sigma_T \propto \frac{\Gamma_i{}^{JT}}{\Gamma_n{}^{JT}}.$$

Thus, for a state (J,n,T) to appear as a resonance, the above quantity must be large. This is expected, for $\Gamma_i{}^{JT}(n)$ is a measure of the probability of populating that state through the entrance channel. Thus, if $\Gamma_i{}^{JT}(n)$ is small, that state is weakly excited. Now, if we compare the states in Table I with the cross section in Fig. 8, we see that the states that show up as resonances are the ones which have a large $\Gamma_i{}^{JT}(n)/\Gamma_n{}^{JT}$. The only exception is the state at 1.369-MeV incident neutron energy, but this state shows up very weakly because it is in the region where the resonance part of the state at 1.2376 interferes destructively with the potential scattering.

There has been some experimental spin assignment[7,20] for the resonances observed with a resolution $\Delta E=125$ keV. To make any correspondence between the experimental spin assignment and the spins predicted by the

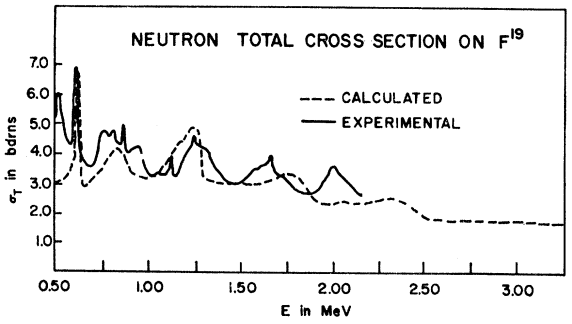

FIG. 7. Calculated and measured total neutron cross section on F^{19}.

[20] A. J. Elwyn (private communication).

TABLE III. Calculated strength function $\langle\Gamma_{lj}{}^J\rangle/\langle D^J\rangle$.

J	$p_{1/2}$	$p_{3/2}$
0	0.0	0.0
1	0.0262	0.0855
2	0.0	0.1386

model, we have averaged our cross section with the same energy interval.

In Table II we have the experimental spin assignment and the spins predicted by the model. We immediately observe that only in some cases do the predicted and measured spins agree. This disagreement could be due to one of two things. First, the single-particle energies we started with were not reliable and if we vary these, we can very easily change the position of the resonances. The only variation we have done is to lower the whole spectrum by 5.35 MeV, which means that the diagonal particle-hole energies were decreased by 5.35 MeV. We did not make any changes in the relative position of the eigenstates H_{QQ}. The second reason for disagreement can be due to the two-particle interaction. We have taken the interaction used by Brown for O^{16}. By varying the two-body interaction, we might be able to change the relative position of these states. However, we do not expect any large change in the position of these states due to changes in the two-body interaction.

The main purpose of this investigation has been to see if the mechanism of simple excitation, in this case particle-hole excitation with rotation, can give us widths of the same order of magnitude as the experimental widths and the right number of resonances. The fact that we have obtained widths of the right magnitude indicates that intermediate-structure resonances can be described in terms of the simple excitations we have chosen. To vary the different parameters in order to try for a better fit to the experiment might be desirable but it is not in the spirit of this investigation.

If we now increase our averaging interval to 0.5 MeV, we see that the resonances disappear and what we get is a flat curve (Fig. 8). However, experimentally, one gets a rather flat curve when the averaging interval is taken to be 0.38 MeV. Comparing our average cross section with the experimental average cross section, we find that the agreement is very good. This agreement between the calculated and observed average cross section indicates that the strength function $\langle\Gamma_\alpha{}^J\rangle/\langle D^J\rangle$ obtained from the model would agree very well with the strength function measured experimentally. In Table III, we present the strength-function evaluated, using Eq. (12) with $\Delta E=2.0$ MeV. Unfortunately, we do not know of any strength-function measurement for this reaction. To get this agreement in the average cross section we must have the right number of resonances, or the right number of degrees of freedom in the system, and the average spacing between the resonances should also be right. The fact that the model has the right number of degrees of freedom indicates that we have to include the collective degrees of freedom into the model. If we try to fit the calculated average cross section with an optical-model potential of the form

$$V(r)=[-V_0-iW]\left[1+\exp\left(\frac{r-R}{a}\right)\right]^{-1}$$

plus a spin orbit term, we find that we can get very good fit with the same parameters V_0, R, and a, used previously, by varying W. The best fit was obtained with $W=1.85$ MeV. This is a very reasonable number for the imaginary part of the optical potential. It indicates that we can get the optical potential, at least the imaginary part of the optical potential, from the shell model we have used, and that this optical potential can reproduce the average observed cross section very well.

Having obtained a rather good agreement in the average neutron cross section, we now turn our attention to the states whose analog states are observed in $n+F^{19}$. These states are $T=1$, $T_3=0$, and are observed in the reaction $F^{19}(p,\gamma_0)Ne^{20}$ and $F^{19}(p,\gamma_1)Ne^{20}$, and can be reached for example in proton scattering from F^{19}. These $T=1$, $T_3=0$ states can however decay by particle emission to both F^{19} and Ne^{19} (see Fig. 1). The width of these $T=1$, $T_3=0$ states is then the sum of neutron and proton width, i.e.,

$$\Gamma_{nK}{}^{J,T=1,T_3=0}=2\pi\{\tfrac{1}{2}\sum_{ljlk}|\langle\Phi_{n,K}{}^{JTT_3}|H_{QP}\times|\psi_{ljlk}{}^{J,T=1,T_3=0}\rangle|_{\text{neutron}}{}^2+\tfrac{1}{2}\sum_{ljlk}|\langle\Phi_{nK}{}^{JTT_3}|H_{QP}\times|\psi_{ljlk}{}^{J,T=1,T_3=0}\rangle|_{\text{proton}}{}^2\}. \quad (35)$$

The factor of $\frac{1}{2}$ comes from the isotopic spin coupling. The difference between the neutron and proton widths is the continuum wave function $V_{lj}(r)$ which appears in the integral F_1.

Before we proceed to evaluate the differential cross section for proton capture, let us look at the relative

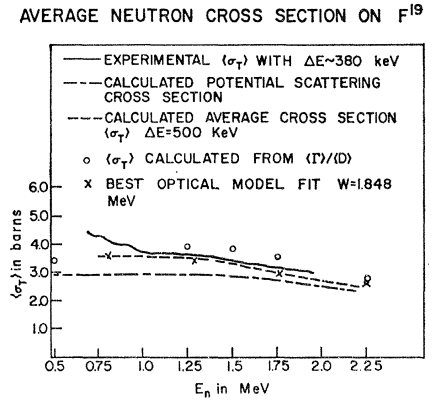

FIG. 8. Calculated average neutron cross section with $\Delta E=0.5$ MeV as compared to the experimental average cross section.

$B(E1)$ strength to the ground state of Ne^{20}. Taking the ground state of Ne^{20} to be a closed shell, and making use of Eqs. (23) and (24), we get for the reduced matrix element of the dipole operator

$$\langle \Phi_{n K}{}^{JTT_3} \| D^1 \| I_i K_i = 0 \rangle = \sum_{\Omega_p q_p \Omega_h q_h} A_{q_p \Omega_p;\ q_h \Omega_h}{}^{K,n} \sum_{l_p j_p l_h j_h} C_{l_p j_p}{}^{q_p \Omega_p} C_{l_h j_h}{}^{q_h - \Omega_h} (-1)^{j_h - \Omega_h}$$

$$\times (-1)^{J+K+\Omega_p+\frac{1}{2}} \left\{ \frac{(2I_i+1)(2J+1)(2j_p+1)(2j_h+1)3}{4\pi} \right\}^{1/2}$$

$$\times \begin{pmatrix} J & 1 & I_i \\ -K & K & 0 \end{pmatrix} \begin{pmatrix} j_p & 1 & j_h \\ -\Omega_p & K & \Omega_h \end{pmatrix} \begin{pmatrix} j_p & 1 & j_h \\ \frac{1}{2} & 0 & -\frac{1}{2} \end{pmatrix} \langle N_p l_p | Cr | N_h l_h \rangle, \quad (36)$$

where C is the strength of the dipole interaction and I_i is the spin of Ne^{20}, which for the ground state is zero. Since the ground state has zero spin, the only eigenstates of H_{QQ} that decay to the ground state of Ne^{20} are the $J=1^-$ states. Due to the fact that our system is deformed, the states $J=1^-$ can be divided into two classes, one with $K=0$, the other with $K=1$. (K is the projection of the total angular momentum along the axis of symmetry.) In Fig. 9, we have the relative $B(E1)$ strength to the ground state of Ne^{20}. The energy is measured relative to the ground state of Ne^{20}. If we look at the $K=1$ and $K=0$ states, we find that the $K=0$ states are at a lower energy than the $K=1$ states. This is in agreement with the hydrodynamic model[21] for a deformed nucleus with positive deformation. However, our microscopic model gives us a strength that is shared among several states.

We now proceed to evaluate the differential cross section for the reactions $F^{19}(p,\gamma_0)Ne^{20}$ and $F^{19}(p,\gamma_1)Ne^{20*}$. The real and imaginary part of the transition amplitude for the above reactions is

$$\mathrm{Re}(T_{\alpha,I}{}^{J,T}) = D_{\alpha,I}{}^{JT} \cos\delta_\alpha + \sum_n \frac{g_\alpha{}^{JT}(n)\gamma_I{}^{JT}(n)}{(E-E_n)^2 + (\frac{1}{2}\Gamma_n{}^{JT})^2}$$

$$\times \{(E-E_n)\cos\delta_\alpha + \tfrac{1}{2}\Gamma_n{}^{JT}\sin\delta_\alpha\}, \quad (37a)$$

$$\mathrm{Im}(T_{\alpha,I}{}^{JT}) = D_{\alpha,I}{}^{JT} \sin\delta_\alpha + \sum_n \frac{g_\alpha{}^{JT}(n)\gamma_I{}^{JT}}{(E-E_n)^2 + (\frac{1}{2}\Gamma_n{}^{JT})^2}$$

$$\times \{(E-E_n)\sin\delta_\alpha - \tfrac{1}{2}\Gamma_n{}^{JT}\cos\delta_\alpha\}, \quad (37b)$$

where $\gamma_I{}^{JT}(n)$ are the reduced matrix elements given by Eq. (36). The $g_\alpha{}^{JT}(n)$ are the same as the $g_\alpha{}^{JT}(n)$ that are used in (34′) for neutrons, except in this case they are for protons, which means that the proton continuum wave function is used to evaluate F_1. δ_α are the proton phase shifts for the incident channel. The matrix elements $D_{\alpha,I}{}^{JT}$ are the reduced matrix elements for direct reaction and are given by

$$D_{\alpha I_i}{}^{JT} = \sum_{l_h j_h, \mu} C_{l_h j_h}{}^{q_h k} F_{l_j, l_h N_h}$$

$$\times \left[(-1)^\mu 3 \left\{ \frac{(2I_i+1)(2j+1)(2j_h+1)}{2\pi} \right\}^{1/2} \right.$$

$$\times \begin{pmatrix} 1 & I_i & 1 \\ \mu & 0 & -\mu \end{pmatrix} \begin{pmatrix} j & \frac{1}{2} & 1 \\ \mu-\frac{1}{2} & \frac{1}{2} & -\mu \end{pmatrix}$$

$$\left. \times \begin{pmatrix} j & j_h & 1 \\ \mu-\frac{1}{2} & \frac{1}{2} & -\mu \end{pmatrix} \begin{pmatrix} j & 1 & j_h \\ -\frac{1}{2} & 0 & \frac{1}{2} \end{pmatrix} \right], \quad (38)$$

where

$$F_{lj,l_h N_h} = C \int_0^\infty V_{lj}(r) R_{N_h l_h}(r) r dr.$$

The total widths $\Gamma_n{}^{JT}$ are given by (35). To evaluate the width, we have to know the open channels. We have taken the six open channels for proton decay, which are defined by the states in F^{19} and used previously in neutron scattering. We also have taken the six states defined by the state of Ne^{19}, which are the analog states to the ones in F^{19}. We thus have a maximum of twelve

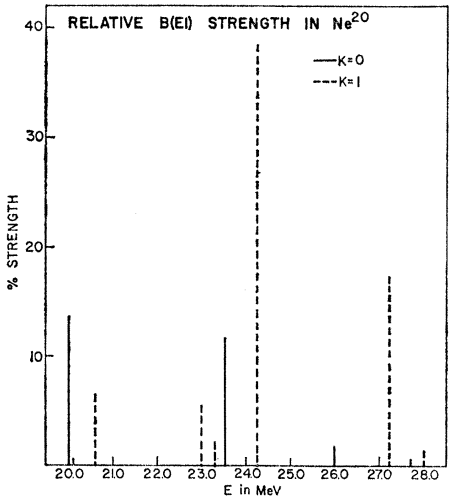

FIG. 9. Relative $B(E1)$ strength in Ne^{20}.

[21] M. Danos and E. G. Fuller, Ann. Rev. Nucl. Sci. 15, 29 (1965).

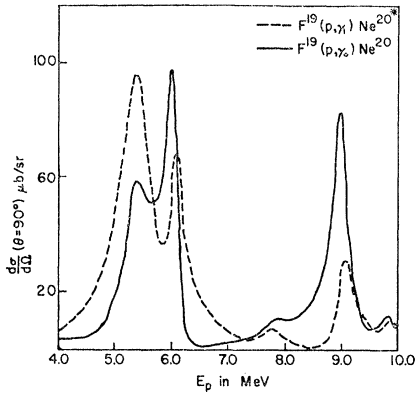

FIG. 10. Calculated differential cross section for $F^{19}(p,\gamma_0)Ne^{20}$ and $F^{19}(p,\gamma_1)Ne^{20*}$.

open channels. As we increase the energy of the incident proton the number of open channels increases up to a maximum of twelve open channels.

Knowing the transition amplitude given by (37a) and (37b), we can evaluate the differential cross section, using Eqs. (16) and (17). This has been done for both $F^{19}(p,\gamma_0)Ne^{20}$ and $F^{19}(p,\gamma_1)Ne^{20*}$, and the results are presented in Fig. 10. In evaluating the above cross section we have shifted the eigenstates of H_{QQ} down by 5.35 MeV as we did with the neutron cross section. We immediately observe that the resonances observed in the γ_0 and γ_1 cross section are at the same energy. This is due to the fact that the only difference in the two processes is the dipole matrix elements. Since Ne^{20} is deformed in the ground state, the first excited state of 2^+ is a rotational band on top of the ground state. Therefore, we have

$$\frac{B(E1;\,1^-\rightarrow 0^+)}{B(E1;\,1^-\rightarrow 2^+)}=\tfrac{1}{2}\text{ for } K=0$$
$$=2\text{ for } K=1.$$

This explains the reason for some resonances having $\sigma_{\gamma_1}/\sigma_{\gamma_0}>1$, while others have $\sigma_{\gamma_1}/\sigma_{\gamma_0}<1$. The reason for having the resonances at the same energy is because they are due to the same eigenstate of H_{QQ}. Comparing the calculated and observed cross section (Fig. 11), we see that the agreement in the position of resonances and the magnitude of the cross section is poor. The reason for the large cross section can be due to the fact that the average field observed by the particle-hole states is not of the same deformation as the ground state. This decreases the overlap between the eigenstates of H_{QQ} and the ground state of Ne^{20}, and thus reduces the magnitude of the cross section. As for the position of the resonances, this could be due to the fact that the single-particle energies we started with were not very good. In Table IV we have the total and elastic widths for all the states between 4.0 and 10.0 MeV incident proton energy, and the relative $B(E1)$ strength for these states. Many of the states in Table IV do not show up as resonances. This is either because Γ_α^J/Γ^J is small or because the relative $B(E1)$ strength is small. Actually, the number of resonances that appears in the calculated cross section is the same as the number of resonances observed experimentally.

Recently,[8] the angular distribution for $F^{19}(p,\gamma_0)Ne^{20}$ and $F^{19}(p,\gamma_1)Ne^{20*}$ has been measured. In Fig. 12 we have the observed and calculated angular distribution. We can see that the calculated angular distribution varies as the energy is increased, while the observed angular distribution remains constant. The constancy in the angular distribution could be due to the fact that one partial wave is feeding the resonances. In that case the angular distribution becomes constant as a function of energy. We have two partial waves feeding the eigenstates of H_{QQ}. They are the $p_{1/2}$ and $p_{3/2}$ partial waves. The only way one of them can dominate is by a coupling through the deformation with the $f_{7/2}$ partial wave. However, the $f_{7/2}$ is weak, until we get to a proton energy of 6 MeV. But his change in the angular distribution with energy is also present below 5 MeV proton energy. This means that the constancy in the angular distribution is not due to coupling through the deformation. If we vary $\gamma_I{}^{JT}(n)$ in the transition amplitude, we notice a remarkable change in the angular distribution. If we assume that $g_\alpha{}^{JT}(n)$ and $\Gamma_n{}^{JT}$ are constant and use the $\gamma_I{}^{JT}(n)$ from experiments, we get an angular distribution such that the cross section at 90° is always larger than the cross section at 0°. However, the ratio

TABLE IV. Energy, spin, elastic width, total width, and $B(E1)$ strength for states in proton capture between 4 and 10 MeV proton energy.

E (MeV)	J	K	Γ_i^J (proton) (keV)	Γ^J (keV)	$B(E1)$ strength
4.817	1	1	32	827	5.6
5.15	1	1	16	365	2.2
5.34	1	0	58	666	11.6
6.05	1	1	7	257.9	38.6
7.77	1	0	9	432	1.8
9.01	1	1	25	352	17.4
9.5	1	0	100	1155	0.6
9.8	1	1	40	368	1.4

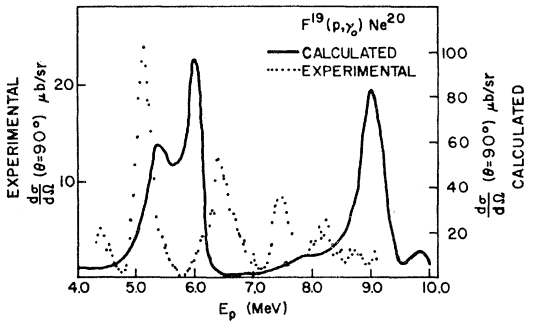

FIG. 11. Calculated and measured differential cross section for $F^{19}(p,\gamma_0)Ne^{20}$.

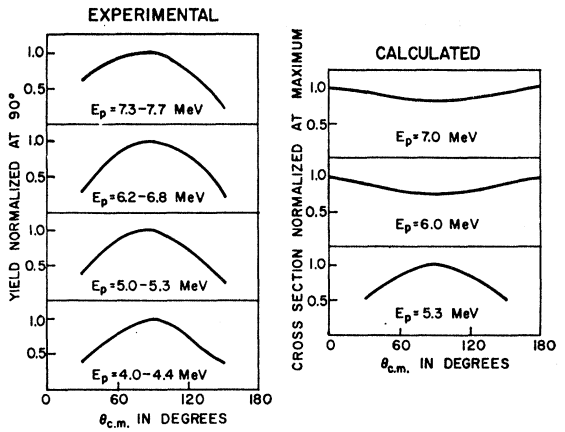

FIG. 12. Calculated and measured (Ref. 17) distribution for $F^{19}(p,\gamma_0)Ne^{20}$.

$(d\sigma/d\Omega)(\theta=90°)/(d\sigma/d\Omega)(\theta=0°)$ varies as the energy changes. This all seems to indicate that the constancy in the angular distribution depends very critically on the choice of the proper $\gamma_I{}^{JT}(n)$, $g_\alpha{}^{JT}(n)$, $\Gamma_n{}^{JT}$, and on their relative magnitude.

The fact that the observed and calculated widths are of the same magnitude indicates that the particle widths have been described reasonably well in our model. Finally, we evaluate the integrated cross section over the energy interval between 3.0 and 10.0 MeV. The experimental integrated cross section comes out to be 41.28 μb MeV/sr, while the calculated integrated cross section is 118 μb MeV/sr. The fact that the calculated integrated cross section is large indicates that the photon widths are too large. This disagreement in the integrated cross section can be due to the assumption that the average field observed by the particle-hole states has the same deformation as the ground state. Taking this deformation to be different will lead to a smaller overlap between the ground state of Ne^{20} and the giant dipole state. This smaller overlap will lead to a smaller γ-ray width, and thus a smaller integrated cross section. Actually, one would expect a change in the deformation of the nucleus at such high excitation. The experimental cross sections for $F^{19}(p,\gamma_0)Ne^{20}$ and $F^{19}(p,\gamma_1)Ne^{20*}$ indicate that $d\sigma/d\Omega(\gamma_1)/d\sigma/d\Omega(\gamma_0)$ increases with increasing energy, indicating that on the basis of the rotational model, $K=0$ states are at a higher energy than the $K=1$ state. This tends to indicate that the giant dipole state might have a negative deformation as compared to the positive deformation of the ground state.

V. CONCLUSION

Our investigation indicates the possibility of understanding the average properties of the intermediate-structure resonances in the $A=20$ system in terms of simple excitation of the compound system. Thus we are able to reproduce the experimental average widths and spacings of the resonances by describing the simple excitation of the compound system in terms of particle-hole states plus rotational bands. The extra degrees of freedom obtained from the rotational motion are essential to give us a reasonable strength function $\langle\Gamma_\alpha{}^J\rangle/\langle D^J\rangle$ and thus the right order of magnitude in the average total cross section (Fig. 8). The success of the model in reproducing the average neutron total cross section ($\Delta E=0.5$ MeV) indicates the feasibility of obtaining a reasonable optical potential from the model, and thus explains from the point of view of dynamics the optical potential in terms of the shell model. The agreement in the widths of the resonances with the experimental widths indicates the smallness of the contribution of more complicated excitations of the compound system (e.g., two-particle–two-hole) to the total widths.

In our model we have assumed that the ground state and excited state (excitation energy of 20 MeV) of Ne^{20} have the same deformation. This can be the reason for obtaining such a large differential cross section for $F^{19}(p,\gamma)Ne^{20}$. Had we taken into consideration the change in deformation with excitation, the overlap between the ground state and excited states would be much smaller. This would lead to smaller γ-ray widths and thus a smaller cross section.

We have observed that the same modes of excitation (i.e., particle-hole plus rotation) gives rise to the observed resonances in the two channels $n+F^{19}$ and $\gamma+Ne^{20}$ that feed the compound system of $A=20$. This stresses the importance of the simple excitation of the compound $A=20$ system, and points to the probability that these resonances are not random fluctuations.

ACKNOWLEDGMENTS

The author wishes to express his gratitude to Professor R. H. Lemmer for suggesting this problem, and for the many inspiring discussions throughout its course. He is also grateful to Professor R. H. Lemmer and Professor B. F. Bayman for reading the manuscript, and he extends his thanks to E. Auerbach for assistance in the programming.